On the density of states of germanium telluride

C. Longeaud, J. Luckas, D. Krebs, R. Carius, J. Klomfass, and M. Wuttig

Citation: Journal of Applied Physics **112**, 113714 (2012);
View online: https://doi.org/10.1063/1.4768725
View Table of Contents: http://aip.scitation.org/toc/jap/112/11
Published by the American Institute of Physics

On the density of states of germanium telluride

C. Longeaud,[1,a)] J. Luckas,[1,2] D. Krebs,[3] R. Carius,[4] J. Klomfass,[4] and M. Wuttig[2,5]
[1]*Laboratoire de Génie Electrique de Paris (CNRS UMR 8507), Plateau de Moulon, 11 rue Joliot Curie, 91190 Gif sur Yvette, France*
[2]*I. Physikalisches Institut IA, RWTH Aachen University, 52056 Aachen, Germany*
[3]*IBM Zurich Research Laboratory, Säumerstrasse 4, 8803 Rüschlikon, Switzerland*
[4]*IEF-5 Photovoltaik, Forschungszentrum Jülich, 52425 Jülich, Germany*
[5]*JARA Fundamentals of Future Information Technology, RWTH Aachen University, 52056 Aachen, Germany*

(Received 22 August 2012; accepted 7 November 2012; published online 11 December 2012)

Germanium telluride (GeTe) is one of the most studied phase change materials. Surprisingly, only little is known about the density of states (DOS) in its band gap. In this paper, the DOS of amorphous GeTe films is investigated both experimentally and theoretically. We propose a model for this DOS as well as estimates of some of the transport parameters of this material. Thin films of amorphous GeTe have been deposited by sputtering. Their dark and photoconductivity have been measured as a function of temperature. By means of the modulated photocurrent technique their DOS was probed, while their absorption was investigated by photothermal deflection spectroscopy at room temperature. Numerical calculations were employed to reproduce the experimental results with a proper set of transport parameters and choice of DOS. These data constitute a good basis for further study on the influence of the DOS on the aging of the sample resistance ("resistance drift").
 [http://dx.doi.org/10.1063/1.4768725]

I. INTRODUCTION

Phase change materials (PCMs) possess attractive properties which are suitable for data storage applications. They can be rapidly and reversibly switched between the amorphous and crystalline states. This phase transformation is accompanied by a pronounced change of optical properties, which is already exploited in rewriteable optical data storage.[1] However, these materials are also very attractive for non-volatile electronic memories, where the pronounced change of electrical resistivity is utilized.[2,3] GeTe is one of the first phase-change materials studied, since its feasibility for rewriteable optical data storage was already verified in 1986.[4] Recently, it was shown, that electrical switching in small GeTe cells can be achieved within a few nanoseconds.[5] This dynamic random access memory (DRAM)-like speed implies that phase-change materials might help to realize a universal memory,[6,7] which combines the switching speed of the DRAM with the non-volatility of the Flash memory. To further increase the application potential of such an electronic memory, it would be highly desirable to realize multilevel storage in phase change memories. While the pronounced contrast in electrical conductivity between the amorphous and crystalline state facilitates multi-level storage, the increase of the resistivity of an amorphous region with time ("resistance drift") endangers the realization of multilevel storage.[8] Hence, it is highly desirable to understand and prevent resistance drift. Recent theories relate resistance drift with the temporal evolution of the density of states (DOS).[9–12] With this goal in mind, we have studied amorphous GeTe (a-GeTe). Recently, we have investigated this compound by means of the modulated photocurrent (MPC) technique.[13] This technique, proposed by Oheda decades ago,[14] is a very powerful tool to investigate the DOS of glassy or semiconductor materials.[15,16] In this paper, we investigate the amorphous GeTe DOS both experimentally and by means of numerical calculations, trying to reproduce the temperature dependence of the dark and photoconductivity as well as the MPC spectra measured for this material. We have also tried to reproduce the dependence of the absorption coefficient on photon energy at room temperature. We describe the procedure we have followed to estimate transport parameters such as the extended states hole mobility μ_p and the equivalent density of states N_v at the valence band edge E_v. From the results of these numerical calculations, we propose a model of amorphous GeTe DOS which includes the distribution of different states as well as their capture coefficients. From this model, we expect to get a better understanding of the DOS in a-GeTe and, further, to investigate the possible link(s) between resistivity and temporal evolution of the DOS.

II. SAMPLES AND EXPERIMENTS

The a-GeTe samples consist of a glass substrate on which a 100 nm or 200 nm thin, amorphous GeTe film, and two parallel rectangular Al ohmic electrodes with a width of 8 mm and a distance of 2 mm apart were deposited subsequently. The a-GeTe deposition process was achieved using an LS 320 von Ardenne Sputter system operating in constant 20–25 W power mode, 20 s.c.c.m. Ar flow, and stoichiometric targets of 99.99% purity. For Fourier transform infrared (FTIR) spectroscopy in reflectance mode, the glass was covered with a 200 nm aluminium film before GeTe deposition. For the photothermal deflection spectroscopy (PDS) measurements, the films were deposited onto Herasil® 102 so as to have the minimum influence of the substrate onto the experimental results.

[a)]E-mail: longeaud@lgep.supelec.fr.

Steady-state dark and photo-conductivity (SSPC) were measured every 10 K between 100 and 300 K on samples fitted onto the cold finger of a dynamically pumped cryostat. The photoconductivity was measured with the sample being illuminated by a constant flux ($F_{dc} = 10^{16}$ cm^{-2} s^{-1}) of infrared light (850 nm). For each measurement, we waited 10 min for the temperature to stabilize and took 20 acquisitions, one each second. The value of the dark and photocurrent was obtained from averaging of these acquisitions, which resulted in an error of less than 5%. The same light was used to perform MPC experiments to determine the DOS. MPC data were measured every 5 or 20 K between 120 and 300 K. The amplitude of the modulated flux was 4 times lower than the average flux F_{dc} and the modulation frequencies were in the range from 12 Hz to 40 kHz. Each measurement was the average of 20 acquisitions of the phase shift and modulus of the alternating current and resulted in an error of the order of 10%. From FTIR measurements, we have deduced the variation of the band gap with temperature T. Reflectance measurements were obtained between 4 and 300 K for photon energies E from 0.04 to 1 eV. The absorption coefficient $\alpha(E)$ was deduced from the analysis of the reflectance spectra by means of a Tauc-Lorentz oscillator model using the software SCOUT.[17] We have defined the band gap as the energy value for which $\alpha(E) = 10^4$ cm^{-1}, known as the E_{04} value. In addition, Seebeck measurements were performed between 220 K and room temperature to derive the position of the Fermi level E_f with respect to the valence band edge E_v.

Finally, PDS has been applied at room temperature to 800 nm thick a-GeTe films, deposited onto Herasil® 102 substrates. From these data, the dependence of the absorption coefficient $\alpha(E)$ on the photon energy E was derived. These variations span typically four orders of magnitude for photon energies in the range $0.4 \leq E \leq 1.2$ eV.

III. EXPERIMENTAL RESULTS

Most of the amorphous GeTe films were found to be poorly photoconductive between 200 and 300 K, with very little difference between the currents measured under dark or illumination. The room temperature dark conductivity was of the order of $\sigma = 5 \times 10^{-4}$ S/cm. From the temperature dependence of σ in an Arrhenius plot, an activation energy of $E_a \approx 0.31$ eV is obtained for $210 \leq T \leq 300$ K (See Fig. 1). For temperatures below 200 K, the Arrhenius plot of σ departs from a straight line. The onset of a hopping contribution to the conductivity could be a possible explanation for this departure.

Despite the poor photoconductivity, it was possible to perform a DOS spectroscopy from the MPC experiment for most of the films. In MPC experiments, the sample is illuminated by a light flux modulated with angular frequency ω, while the induced alternating photo current is measured. It was shown[15,16] that from these experimental data, i.e., modulus of the alternating photocurrent and its phase shift ϕ with respect to the excitation light, one can deduce the quantity NC_p/μ_p, that we shall call MPC-DOS in the following. N denotes the density of states at an energy E_ω and C_p the capture coefficient of the states trapping free carriers (holes in a-GeTe, hence the index p). Following[15,16] the MPC-DOS is derived via the equation,

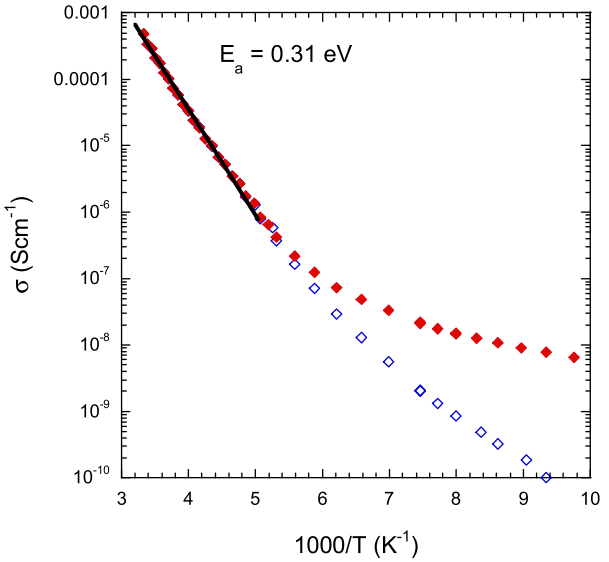

FIG. 1. Typical dark (open diamonds) and photo + dark (full diamonds) conductivity of amorphous GeTe films. An activation energy of $E_a = 0.31$ eV is obtained from fitting the highest temperatures data of dark conductivity (solid black line).

$$\frac{N(E_\omega)C_p}{\mu_p} = \frac{2}{\pi k_B T} q G_{ac} \frac{\sin\phi}{|\sigma_{ac}|} \tag{1}$$

with

$$E_\omega - E_v = k_B T \ln\left(\frac{C_p N_v}{\omega}\right), \tag{2}$$

where k_B is the Boltzmann constant, q the electron charge, and $|\sigma_{ac}|$ the modulus of the alternating photoconductivity resulting from modulated generation rate G_{ac}. From Eq. (2), it can be seen that the energy E_ω of the probed states can be varied and chosen by changing either the temperature or the angular frequency. All the quantities on the right hand side of Eq. (1) being known, Eqs. (1) and (2) would offer an easy DOS spectroscopy by varying T and ω. However, C_p, μ_p, and N_v are unknown. In addition, Eq. (2) assumes that the band gap of a-GeTe is temperature independent. Therefore, E_v is considered as constant for all the measurement temperatures and is implicitly used as a zero for the energy scaling. Nonetheless, FTIR measurements reveal that the band gap varies with temperature following the equation:

$$E_{04}(T) = E_{04}(T = 0\,\text{K}) - \xi T^2, \tag{3}$$

where ξ is $\approx 1.3 \times 10^{-6}$ eV/K^2 and $E_{04}(T = 0\,\text{K}) \approx 0.95$ eV. Finally, Seebeck measurements have shown that this evolution of the gap was essentially due to a movement of the valence band edge with regard to a fixed conduction band edge. Therefore, we have corrected Eq. (2) by taking into account the temperature dependence of the band gap in order to define the same zero for the energy scaling at all the measurement temperatures. A detailed description of this procedure is presented in Ref. 18. Fig. 2 displays typical NC_p/μ_p spectroscopy

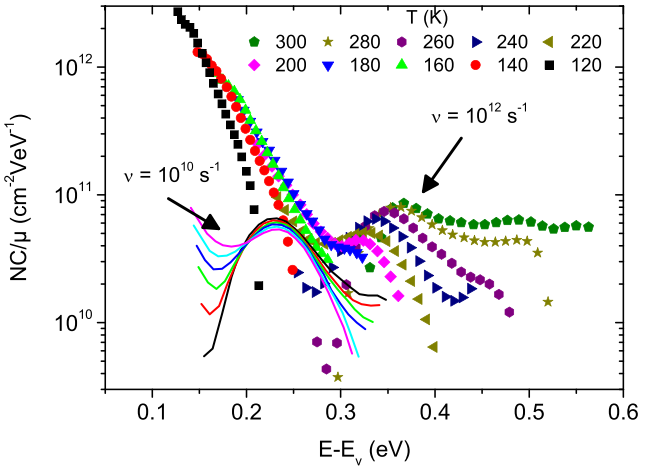

FIG. 2. NC_p/μ_p vs energy of an a-GeTe film corrected for temperature variation of the band gap. The spectra obtained at the temperatures indicated in the figure are plotted either with $\nu = 10^{12}\,s^{-1}$ (symbols) or with $\nu = 10^{10}\,s^{-1}$ (lines for temperatures in the range 220–250 K in 5 K steps). The error bars are within the size of a symbol.

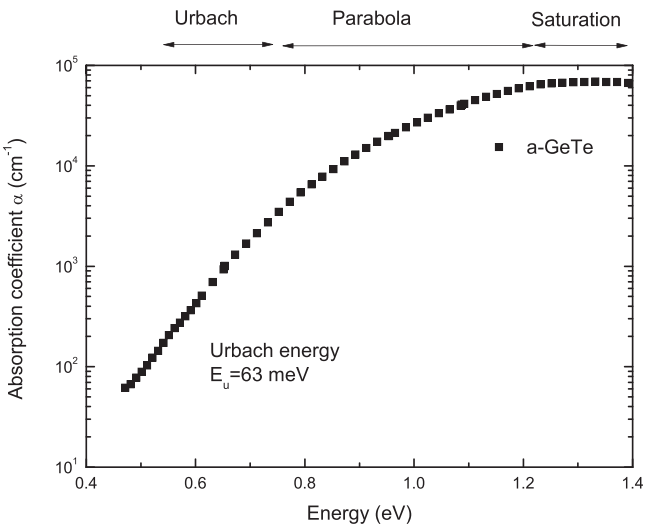

FIG. 3. Typical dependence of the absorption coefficient on the photon energy measured by PDS on an amorphous GeTe film.

data, corrected for the band gap variations, we have obtained for one of the a-GeTe films studied. It can be seen that the MPC-DOS consists of a band tail along with some deep states, one of which presents a rather well defined bell shape. In this figure, each of the presented spectra is calculated applying Eqs. (1) and (2) to the MPC data obtained at varied temperature T and angular frequency ω. One spectrum consists in data sets (symbols) measured at constant temperature T by varying the excitation frequency ω from 12 Hz to 40 kHz. According to Eq. (2), data points within any one data set scale closer to the valence band for $\omega = 40$ kHz, whereas data points taken with lower frequency scale closer to mid gap. The choice of consecutive temperatures was such that the energy range scanned at one temperature by varying the frequency has a significant overlap with the energy range scanned at the next temperature. In this way, assuming that the technique is probing one type of states in a given range of temperatures, a "type" of states being defined by its single common capture coefficients, the MPC spectra obtained at consecutive temperatures must match one another by a proper choice of the attempt-to escape frequency $\nu = C_p N_v$.

To obtain the complete spectra shown in Fig. 2 from the MPC raw data (phase and modulus), we had to assume different values for the attempt-to escape frequency $\nu = C_p N_v$. In the case of the valence band tail (VBT), probed at low temperature, a 20-K step was enough to achieve a good match with $\nu = C_p N_v = 10^{12}\,s^{-1}$. It can be seen that the parts of the spectra obtained at high frequency, i.e., the parts closest to the valence band edge, are all converging in a single envelope describing an exponentially decreasing valence band tail. With a higher ν, these parts would not match, and, with a lower ν the spectra would have crossed. The fact that at low frequency the spectra depart from the upper envelope can be due to the influence of the mean dc flux as demonstrated in a previous paper.[15] In the case of the "bell-shaped" state around 0.25 eV, we had to perform measurements each 5 K between 220 and 250 K and to choose $\nu = 10^{10}\,s^{-1}$ to obtain the best match for the MPC spectra displayed in Fig. 2 (Full lines). Indeed, it is only in this small range of temperature that this peak can be probed and observed. In this range, all spectra exhibited a clear maximum that we assumed to correspond to the maximum of the probed distribution of states. An adjustment of this maximum at the same energy position was only possible with $\nu = 10^{10}\,s^{-1}$. Unfortunately, we were unable to estimate a ν value for the deepest states above 0.35 eV for which no particular shape is visible. That is why they are plotted with the same ν as the VBT though their capture coefficient(s) and, hence their ν, is (are) probably different.

While the MPC technique is able to observe the DOS between valence band and Fermi level, information about the DOS above the Fermi level can be obtained by a combination with absorption measurements which are probing a convolution of occupied and unoccupied states. In Fig. 3, the dependence of the absorption coefficient $\alpha(E)$ on photon energy as measured by photothermal deflection spectroscopy is depicted.[19,20] Three regions can be seen in this graph. At low photon energy an exponential dependence of $\alpha(E)$ is visible, from which we extract an Urbach energy $E_u = 63$ meV corresponding to the contribution of band tails to the absorption. For higher energies, the dependence of $\alpha(E)$ follows a parabola corresponding to the contribution of the band edges, while for even higher energies, a saturation is reached when all the photons are absorbed in the layer independently of their energy. In this saturation region, no information on the DOS can be gained.

IV. DISCUSSION

To obtain more insight into the transport and DOS parameters, we have developed numerical calculation software reproducing the SSPC and MPC experiments. This software, DeOSt, is available on the web site of the LGEP.[21] The user can define the parameters of the DOS (width of band gap, mobility, DOS distributions, capture coefficients,…) and introduce "experimental" parameters (flux, frequency of the modulation, temperature,…). The software calculates the data (dc and ac currents, phase shift,…). Subsequently, the

computed results can be compared with experimental results. Some of the parameters introduced come directly from experimental measurements, such as the band gap width (FTIR, PDS), the Fermi energy E_f (Seebeck, SSPC), the slope of the valence band tail, and some ν values (MPC). Others are adjusted to obtain the experimental trends observed in SSPC, MPC, and PDS.

For the film studied, we found from steady state photoconductivity (SSPC) a position of the dark Fermi level E_f of 0.31 eV measured from activation of the dark conductivity. Since photoconductivity is low down to temperatures around 180 K, the mid gap density of states must be high, and thus limiting the splitting of the quasi Fermi levels.

Knowing the position of the dark Fermi level, the value of the dark conductivity, gives some indications on the product $\mu_p N_v$. We have found a dark conductivity at room temperature of the order of $\sigma = 5 \times 10^{-4}$ S/cm. If we write

$$\sigma = q\mu_p p = q\mu_p N_v \exp\left(\frac{E_v - E_f}{k_B T}\right), \tag{4}$$

we derive an order of magnitude of $\mu_p N_v \approx 10^{21}\,\mathrm{cm^{-1}\,V^{-1}\,s^{-1}}$ taking for E_v-E_f the value of the activation energy, i.e., $E_a = 0.31$ eV.

Since amorphous GeTe is a P type material, the band tail we find in MPC is very likely the valence band tail. If we assume from the experimental results that this band tail is exponentially decreasing from the valence band edge following an equation:

$$N(E) = N_{v0} \exp\left(\frac{E_v - E}{k_B T_v}\right), \tag{5}$$

we can estimate the value of T_v to be $T_v \approx 350$–380 K ($k_B T_v \approx 30$–33 meV). As mentioned before, the best matching between the different spectra of the MPC experiment measured at different temperatures is obtained for an attempt to escape frequency $\nu = C_p N_v \approx 10^{12}\ \mathrm{s^{-1}}$. Thus, we can deduce the ratio $C_p/\mu_p \approx \nu/(\mu_p N_v) \approx 10^{-9}$ cm/V. The NC/μ values are completely determined from MPC data (see Eq. (1)). Then, if we consider these data for E - $E_v = 0.2$ eV, one obtains $N(0.2)C_p/\mu_p \approx 5 \times 10^{11}\,\mathrm{cm^{-2}\,eV^{-1}}$ V. If we assume $k_B T_v \approx 33$ meV, it follows $N_{v0} \approx 2 \times 10^{23}\,\mathrm{cm^{-3}\,eV^{-1}}$. Since $N_v \approx k_B T N_{v0}$, we obtain $N_v \approx 5 \times 10^{21}\,\mathrm{cm^{-3}}$ which results in $\mu_p \approx 0.2\ \mathrm{cm^2\ V^{-1}\ s^{-1}}$ and $C_p \approx 2 \times 10^{-10}\ \mathrm{cm^3\ s^{-1}}$.

In this way, we can derive important transport parameters from conductivity and MPC measurements such as the position of the dark Fermi level ($E_f \approx 0.31$ eV), the hole extended states mobility ($\mu_p \approx 0.2\ \mathrm{cm^2\ V^{-1}\ s^{-1}}$), the equivalent density of states at the valence band edge ($N_v \approx 5 \times 10^{21}\,\mathrm{cm^{-3}}$), the characteristic energy of the valence band tail ($k_B T_v \approx 30$–33 meV), and the hole capture coefficient of these states ($C_p \approx 2 \times 10^{-10}\ \mathrm{cm^3\ s^{-1}}$).

Now, we can use the PDS measurements to deduce some information on the conduction band tail (CBT). Indeed, the Urbach energy obtained on this sample is $E_u = 63$ meV. This Urbach energy is the convolution of all the possible optical transitions from the full states below the Fermi level towards the empty states above it following the equation:

$$\alpha(\hbar\omega_{ph}) = \int C_{opt} N(E) f(E) \times C_{opt} N(E + \hbar\omega_{ph}) \times \left(1 - f(E + \hbar\omega_{ph})\right) \frac{dE}{\hbar\omega_{ph}}, \tag{6}$$

where $f(E)$ is the occupation function, C_{opt} the optical coefficients, and $\hbar\omega_{ph}$ the photon energy. If different types of states are present, this integral has to be extended to all these states taking account of the proper optical coefficient for each state. Since the MPC experiment suggests a characteristic energy for the valence band tail of around 33 meV, the characteristic energy of the CBT is probably much larger, at least around 60 meV, to obtain the observed Urbach energy of 63 meV.

In Fig. 4(a), a first possibility for the a-GeTe DOS is presented defined by means of the parameters deduced above, trying also to fit the absorption data as displayed in Fig. 3. One can see that the dark Fermi level at 300 K (vertical line) is fixed by the two band tails around 0.25 eV above the valence band edge. The characteristic temperature of the VBT

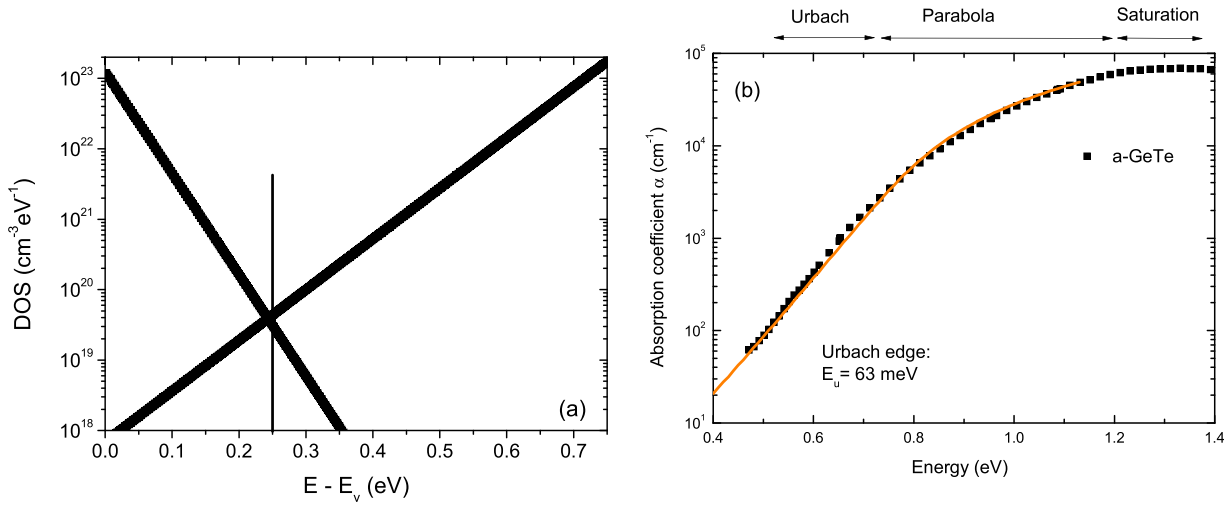

FIG. 4. (a) a-GeTe DOS made of two band tails which fix the Fermi level, indicated by a vertical line, at 0.25 eV above E_v. (b) A fit (full line) of the experimental variations (symbols) of the absorption coefficient measured by PDS.

is 350 K ($k_BT_v = 30$ meV) and the characteristic temperature of the CBT is $T_c = 700$ K ($k_BT_c = 60$ meV) with a band gap width of 0.75 eV.

The chosen DOS gives an excellent agreement between calculated and experimental PDS data as shown in Fig. 4(b). Before going further, we would like to comment on the PDS spectra and the chosen density of states. The DOS derived in Fig. 4(a) does not correspond to the early proposition of Bahl and Chopra.[22,23] These authors had suggested that the VBT could be larger than the CBT which is the opposite of the proposed solution. However, they underlined that their proposal was only schematic due to the lack of information at that time. To have a P type material implies a VBT smaller than the CBT, in the absence of additional donor or acceptor type states, for simple neutrality reasons. The good agreement between the experimental and calculated PDS spectra in Fig. 4(b) was obtained for a value of the optical coefficient $C_{opt} = 8 \times 10^{-22}$ cm$^{5/2}$ eV, which was taken, to be the same for both band tails and the extended states. Hence, the order of magnitude of the optical coefficients can be estimated after comparison of the results of SSPC, MPC, and PDS. Finally, we have chosen for simplicity reasons $N_c = N_v$ but lack information to verify this assumption.

While the calculated and experimental absorption coefficients agree very well as shown in Fig. 4(b), the calculated dark conductivity at room temperature is 7×10^{-3} S/cm, which is 10 times higher than the measured value. This deviation arises from a Fermi level being fixed too close to the valence band. In addition, the calculated MPC spectra using the DOS displayed in Fig. 4(a) reveal a steadily decreasing band tail without any of the structures observed experimentally in the range 0.35–0.55 eV above E_v. Therefore, the introduced DOS has to be refined to produce results closer to the experimental ones.

Since we observe a peak around 0.25 eV in MPC, we have added a peak of states 0.25 eV above E_v. These states are likely to be of donor type shifting the Fermi level towards the experimentally observed energy position from the valence band. Experimentally, the peak is well described, i.e., the MPC spectra taken at different temperatures converge well, with an attempt to escape frequency of $\nu_p \approx 10^{10}$ s^{-1}, resulting in a capture coefficient of the order of $C_p \approx 2 \times 10^{-12}$ cm^3 s^{-1}. From the NC/μ value at the maximum, we estimate $N_{max} \approx 10^{22}$ cm^{-3} eV^{-1}. The reader should note that the bump experimentally observed in Fig. 2 around 0.35 eV for the spectra plotted with $\nu = 10^{12}$ s^{-1} (symbols) is linked to a contribution of the "bell shape" state to the MPC signal plotted with the wrong ν. Indeed, these spectra were recorded in the same range of temperature ($220 \leq T \leq 260$ K) in which we can describe properly the "bell shape" state at 0.25 eV with $\nu = 10^{10}$ s^{-1} ($220 \leq T \leq 250$ K). That is why the addition to the DOS of Fig. 4(a) of a peak of states 0.25 eV above E_v, as displayed in Fig. 5(a), gives rise to the bump observed around 0.35 eV in Fig. 5(b) in which the MPC spectra were scaled with $\nu = 10^{12}$ s^{-1}.

The dark Fermi level at 300 K is located deeper in the gap, 0.33 eV above E_v, compared to the previous distribution of Fig. 4(a), but this DOS is still not satisfying because the dark Fermi level is not well pinned, i.e., it moves a lot with temperature, coming closer to the valence band as the temperature decreases. The value of the dark conductivity at 300 K would be correct but, due to the movement of the Fermi level the activation energy is too low, of the order of 0.27 eV instead of the experimental value of 0.31 eV. Besides, the calculated MPC DOS does not resemble the experimental one (See Fig. 5(b)) since the deepest states do not extend very far into the gap, that is beyond 0.45 eV, with values of the MPC-DOS of the order of a few 10^{10} cm^{-3} eV^{-1} as observed experimentally.

The only way to obtain a DOS with a deep states contribution beyond 0.45 eV above the valence band is to add at least one acceptor distribution above the Fermi level as shown in Fig. 6. However, the applied analysis procedure given by Eqs. (1) and (2) is only valid for full states when applied to a P type material. Hence, the distribution of states in the energy range above the dark Fermi level cannot be reproduced correctly using Eq. (1). As a consequence, the simulated MPC signal can be very different from the implemented density of states in this energy region. Thus, even though an acceptor state above the Fermi level may have a

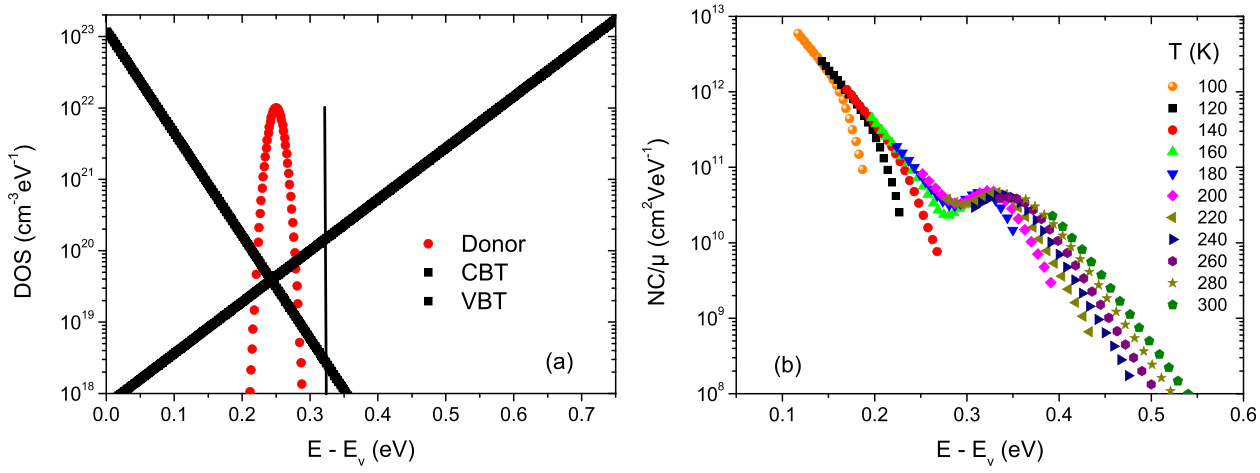

FIG. 5. (a) Refinement of the DOS of Fig. 4(a) by addition of deep donor states that moves the Fermi level, indicated by a vertical line, to a more "reasonable" position. (b) The MPC-DOS calculated with the DOS of Fig. 5(a) and scaled with $\nu = 10^{12}$ s^{-1}.

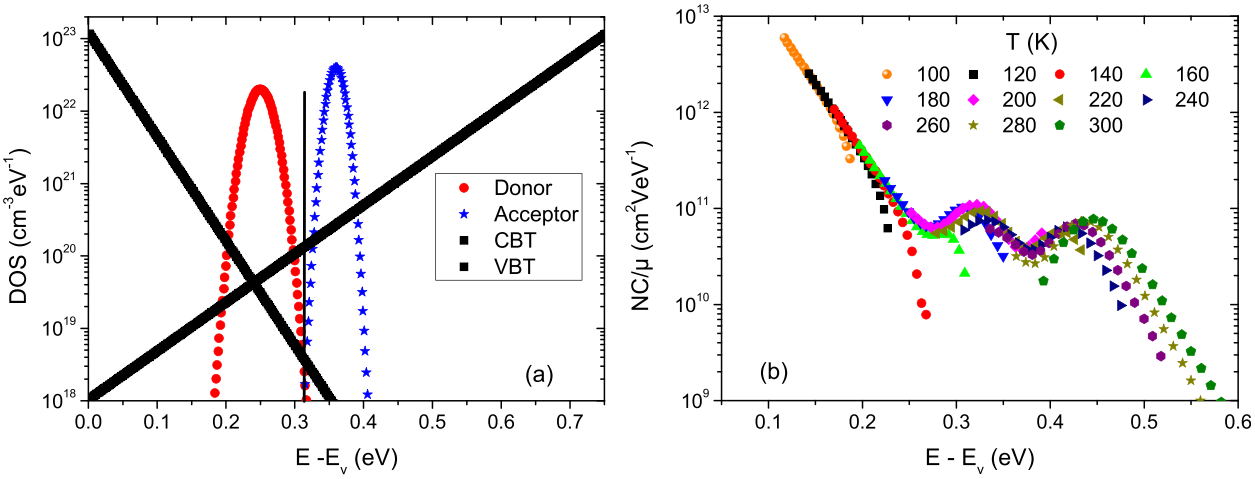

FIG. 6. (a) a more refined DOS that includes deep states, donors and acceptors, pinning the dark Fermi level (vertical line). (b) MPC-DOS plotted from the result of the MPC calculation taking account of the DOS displayed in (a).

significant influence on the simulated MPC spectra, its real shape will not be correctly reproduced by the simulation.

The reproduction of the MPC experimental results with the DOS displayed in Fig. 6(a) leads to the results shown in Fig. 6(b) where it can be seen that the addition of an extra peak of acceptor states above the Fermi level at 0.37 eV from E_v does lead to the emergence of the feature observed at high energy (≈0.45 eV) in the MPC spectra. It can be seen that the MPC simulation does not directly reflect the acceptor peak added at 0.37 eV. The first reason is linked to the above explanation as illustrated in Fig 6. Fig. 6(a) shows the density of states implemented into the simulation with $N_{don} = 2 \times 10^{22}\,\mathrm{cm}^{-3}\,\mathrm{eV}^{-1}$ and $N_{acc} = 4 \times 10^{22}\,\mathrm{cm}^{-3}\,\mathrm{eV}^{-1}$. Despite $N_{acc} > N_{don}$, the simulated Nc/μ values describing the deep acceptor states are lower than those describing the shallow donor state, see Fig. 6(b). This simulation result nicely demonstrates that the density of states above the Fermi level E_f is underestimated by Eq. (1). The second reason is that the MPC spectra of Fig. 6(b) were plotted as we did experimentally with an energy scaling based on $\nu = 10^{12}\,\mathrm{s}^{-1}$, a value that does not correspond to the attempt-to-escape frequency of the introduced acceptor states, and this mismatch results in the appearance of the acceptor states contribution around 0.45 eV instead of 0.37 eV. Nevertheless, the simulated MPC-DOS displayed in Fig. 6 is close to the experimental one, though a clear gap around 0.37 eV exists in the simulated MPC spectrum, from which shallow donors could be clearly distinguished from deep acceptor states. This gap is not observed experimentally, see Fig. 2.

That is why we have introduced another acceptor state, the contribution of which fills the gap in between the donor states contribution and the previously introduced acceptors states, to refine the agreement between calculated and experimental MPC-DOS. To match as accurately as possible, the experimental results of some parameters had to be adjusted slightly but the main trends remained. The DOS depicted in Fig. 7 leads to the MPC spectra presented in Fig. 8, the Arrhenius plot for conductivity and photoconductivity (Fig. 9) and the PDS spectra (Fig. 10).

One can see that the agreement between calculations and experiments is rather good except for the dark conductivity at temperatures below 250 K, where hopping transport may have a significant influence on the transport channel. At low temperature, hopping is also present under illumination

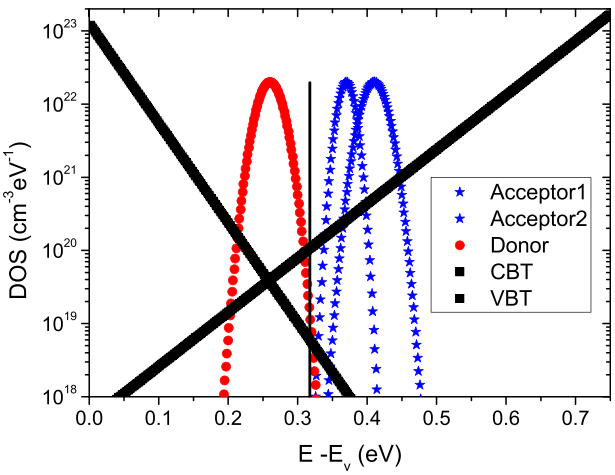

FIG. 7. Density of states introduced in the simulation to reproduce the experimental results of the SSPC, MPC and PDS techniques.

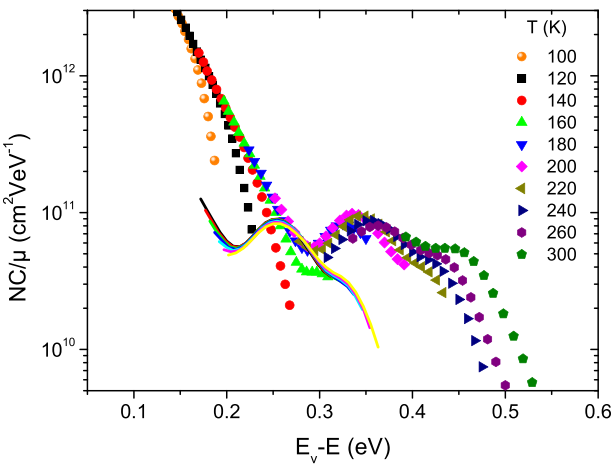

FIG. 8. MPC spectra calculated from the DOS presented in Fig. 7. The spectra depicted by symbols were calculated at the temperatures shown in the figure and plotted with $\nu = 10^{12}\,\mathrm{s}^{-1}$. The spectra depicted by lines were calculated for temperatures in the range 210–250 K and plotted with $\nu = 10^{10}\,\mathrm{s}^{-1}$.

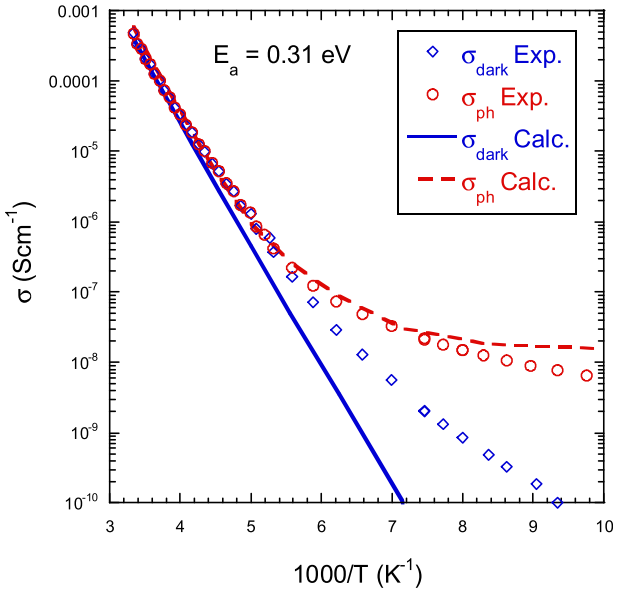

FIG. 9. Arrhenius plot of experimental (symbols) and calculated (lines) variations of the dark σ_{dark} and photo conductivity σ_{ph}.

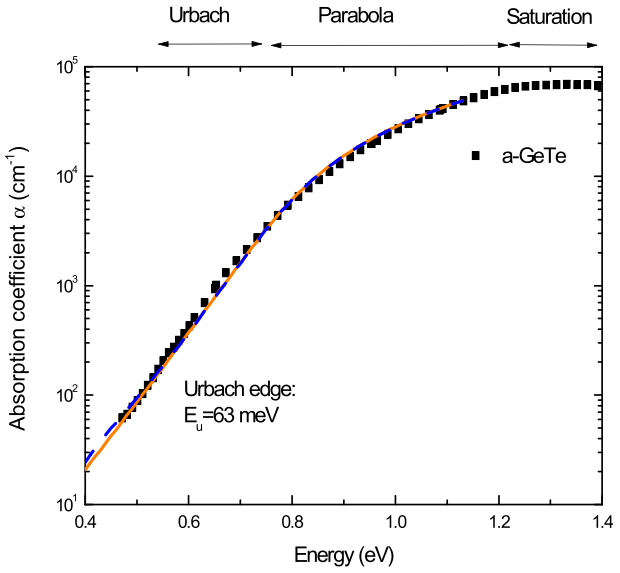

FIG. 10. Fit of the PDS spectrum: with the complete DOS (dashed line), with only the band tails (full line).

but its influence is smaller than under dark. Indeed, the total current is the contribution of both free and hopping carriers. Under dark at low temperature, the free carrier concentration is small and hopping transport gives the major contribution to the current. Hence the disagreement between experimental and calculated data for hopping is not taken into account in the calculation. Under illumination, the free carrier concentration is much higher and its contribution to the current is predominant. It is why, though hopping is not taken into account in the numerical calculation, we have a good agreement between calculated and experimental conductivity behaviors under light.

One point that deserves further explanation is the contribution of the deep states to the PDS spectra. If we had taken the same optical coefficients, as for the band tails, they would have been seen in the PDS spectra as a large bump around 0.6 eV. Since it is not the case, we have assumed that the optical capture coefficients for these states were smaller than for the tails and extended states. Taking values approximately 40 times lower leads to the agreement displayed in Fig. 10. Consequently, these values would be the maximum ones for the deep states optical capture coefficients.

The data we have used in our numerical calculations are given in Table I. The parameters, which were deduced from experimental results, are displayed in bold characters. The other parameters have been adjusted to obtain the best match between calculated and experimental results for the three experiments considered. The reader may note that some of these parameters have only little influence on the final results. For instance, the extended states electronic mobility, that we have taken to be very low to keep the P type nature of the material, can be as large as 0.1 $cm^2\ V^{-1}\ s^{-1}$ without modifying the final results. It cannot be much larger otherwise the material would turn to be N type. The inequalities in Table I give the range in which some parameters may vary without changing the final results, the other parameters being kept constant.

The fact that there is not a single set of parameters to obtain a final agreement between calculated and experimental results show that the model we have developed is probably not the unique solution. For instance, we have used two acceptor state distributions to improve the fitting of the MPC results but the influence of the second distribution of

TABLE I. Data introduced in the numerical calculation to reproduce the experimental results of SSPC, MPC, and PDS techniques. Values indicate upper limits or assumptions made due to a lack of information, the remaining bold values are determined directly from experiments.

Conduction band tail	$T_c = \mathbf{680}$ K ($k_BT_c = 59$ meV) $N_{c0} = 1.7 \times 10^{23}\ cm^{-3}\ eV^{-1}$ $C_{nCBT} = 5.0 \times 10^{-11}\ cm^3\ s^{-1}$ $C_{pCBT} = 5.0 \times 10^{-12}\ cm^3\ s^{-1}$ $C_{optCBT} = 8.5 \times 10^{-22}\ cm^{5/2}\ eV$
Valence band tail	$T_v = \mathbf{370}$ K ($k_BT_v = 32$ meV) $N_{v0} = \mathbf{1.3 \times 10^{23}}\ cm^{-3}\ eV^{-1}$ $C_{nVBT} \leq 5.0 \times 10^{-10}\ cm^3\ s^{-1}$ $C_{pVBT} = \mathbf{5.0 \times 10^{-10}}\ cm^3\ s^{-1}$ $C_{optCBT} = 8.5 \times 10^{-22}\ cm^{5/2}\ eV$
Acceptors 1	$N_{acc1} = 2.0 \times 10^{22}\ cm^{-3}\ eV^{-1}$ $E_{acc1} - E_v = 0.41$ eV $\sigma_{acc1} = 15$ meV $7.0 \times 10^{-13} \leq C_{nacc1} \leq 3.0 \times 10^{-12}\ cm^3\ s^{-1}$ $C_{pacc1} = 3.0 \times 10^{-11}\ cm^3\ s^{-1}$ $C_{optacc1} = 2.0 \times 10^{-23}\ cm^{5/2}\ eV$
Acceptors 2	$N_{acc2} = 2.0 \times 10^{22}\ cm^{-3}\ eV^{-1}$ $E_{acc2} - E_v = 0.37$ eV $\sigma_{acc2} = 10$ meV $5.0 \times 10^{-13} \leq C_{nacc2} \leq 1.0 \times 10^{-12}\ cm^3\ s^{-1}$ $C_{pacc2} = 2.0 \times 10^{-13}\ cm^3\ s^{-1}$ $C_{optacc2} = 2.0 \times 10^{-23}\ cm^{5/2}\ eV$
Donors	$N_{don} = \mathbf{2.0 \times 10^{22}}\ cm^{-3}\ eV^{-1}$ $E_{don} - E_v = \mathbf{0.26}$ eV $\sigma_{don} = 15$ meV $C_{ndon} \leq 5.0 \times 10^{-11}\ cm^3\ s^{-1}$ $C_{pdon} = \mathbf{2.5 \times 10^{-12}}\ cm^3\ s^{-1}$ $C_{optdon} = 2.0 \times 10^{-23}\ cm^{5/2}\ eV$
Other parameters	$E_g(300\text{ K}) = \mathbf{0.75}$ eV; $\mu_{n0} \leq 0.1\ cm^2\ V^{-1}\ s^{-1}$; $\mu_{p0} = \mathbf{0.2}\ cm^2\ V^{-1}\ s^{-1}$; $N_c = 3.9 \times 10^{21}\ cm^{-3}$; $N_v = \mathbf{3.9 \times 10^{21}}\ cm^{-3}$

acceptors onto the other "experiments" is rather limited. This extra distribution should be considered more as a refinement of the results obtained with the two basic distributions of acceptors and donors than a definite result. However, the model we developed gives a general picture consistent with the results of several experiments.

One may note also that we have chosen to model the deep states with monovalent states, even though other types of states are possible, too. Indeed, it was shown that in some chalcogenides, such as As_2Se_3, deep states consist of amphoteric states with negative correlation energy. We have chosen to represent deep states with monovalent states for several reasons. First, the processes of trapping/emission and recombination are far easier to understand with monovalent states. Second, even amphoteric states can be modeled as distributions of monovalent states. Finally, to our knowledge there is no evidence that amphoteric states are present in a-GeTe.[24]

V. CONCLUSION

We have performed SSPC, MPC, and PDS experiments on amorphous GeTe films deposited by sputtering. From these experiments, we have derived estimates for some of the transport and DOS parameters of a-GeTe. Introduced as a starting point in a numerical calculation, these parameters helped us to derive a final set of parameters from which the main trends of SSPC, MPC, and PDS results are consistently reproduced. As expected, the DOS is essentially made of two large band tails, a signature of the disorder usually encountered in amorphous material. Deep states around mid gap have to be added to these two band tails to account for the DOS distribution observed with the MPC technique and to explain the low photocurrent. Values for the capture coefficients of these states have been proposed as well as for the extended states hole mobility. This first attempt to determine the a-GeTe transport and DOS parameters constitutes a good basis for further investigations on a possible link between DOS and drift of resistivity of the amorphous phase of this material.

ACKNOWLEDGMENTS

This work was partly supported by a Procope project (#21870VB) funded by Egide as well as the SFB 917 ("Nanoswitches"). D. Krebs would like to thank Haris Podzidis and Evangelos Eleftheriou for their support of this work.

[1]M. Wuttig and N. Yamada, Nat. Mater. **6**, 824–832 (2007).
[2]B.S. Lee, J. R. Abelson, S. G. Bishop, D. H. Kang, B. K. Cheong, and K. B. Kim, J. Appl. Phys. **97**, 093509 (2005).
[3]I. Friedrich, V. Weidenhof, W. Njoroge, P. Franz, and M. Wuttig, J. Appl. Phys. **87**, 4130 (2000).
[4]M. Chen, K. A. Rubin, and R. W. Barton, Appl. Phys. Lett. **49**, 502–504 (1986).
[5]G. Bruns *et al*., Appl. Phys. Lett. **95**, 043108 (2009).
[6]M. H. R. Lankhorst, B. W. S. Ketelaars, and R. A. M. Wolters, Nat. Mater. **4**, 347 (2005).
[7]M. Wuttig, Nat. Mater. **4**, 265 (2005).
[8]M. Boniardi *et al*., J. Appl. Phys. **105**, 084506–084511 (2009).
[9]D. Ielmini, S. Lavizzari, D. Sharma, and A. L. Lacaita, Appl. Phys. Lett. **92**, 193511 (2008).
[10]D. Ielmini, D. Sharma, S. Lavizzari, and A. L. Lacaita, IEEE Trans. Electron. Devices **56**, 1070 (2009).
[11]A. Pirovano, A. L. Lacaita, F. Pellizzer, S. A. Kostylev, A. Benvenuti, and R. Bez, IEEE Trans. Electron. Devices **51**, 714 (2004).
[12]D. Krebs, R. M. Schmidt, J. Klomfass, J. Luckas, G. Bruns, C. Schlockermann, M. Salinga, R. Carius, and M. Wuttig, J. Non-Cryst. Solids **358**, 2412 (2012).
[13]J. Luckas, D. Krebs, M. Salinga, M. Wuttig, and C. Longeaud, Phys. Status Solidi C **7**, 852–856 (2010).
[14]H. Oheda, J. Appl. Phys. **52**, 6693 (1981).
[15]C. Longeaud and J. P. Kleider, Phys. Rev. B **45**, 11672 (1992).
[16]R. Brüggemann, C. Main, J. Berkin, and S. Reynolds, Philos. Mag. B **62**, 29–45 (1990).
[17]W. Theiss, http://mtheiss.com/.
[18]J. Luckas, S. Kremers, D. Krebs, M. Salinga, M. Wuttig, and C. Longeaud, J. Appl. Phys. **110**, 013719 (2011).
[19]A. C. Boccara, D. Fournier, and J. Badoz, Appl. Phys. Lett. **36**, 130–132 (1980).
[20]W. B. Jackson, N. M. Amer, A. C. Boccara, and D. Fournier, Appl. Opt. **20**, 1333–1344 (1981).
[21]C. Longeaud, http://www.lgep.supelec.fr/index.php?page=scm-logiciels.
[22]S. K. Bahl and K. L. Chopra, J. Appl. Phys. **41**, 2196–2212 (1970).
[23]S. K. Bahl and K. L. Chopra, J. Appl. Phys. **40**, 4940–4947 (1969).
[24]J. Robertson, K. Xiong, and P. W. Peacock, Thin Solid Films **515**, 7538–7541 (2007).